



UNIVERSITY OF LEEDS

This is a repository copy of *Crystal structure, recombinant expression and mutagenesis studies of the bifunctional catalase-phenol oxidase from Scytalidium thermophilum*.

White Rose Research Online URL for this paper:  
<http://eprints.whiterose.ac.uk/81757/>

---

**Article:**

Yuzugullu, Y, Trinh, CH, Smith, MA et al. (6 more authors) (2013) Crystal structure, recombinant expression and mutagenesis studies of the bifunctional catalase-phenol oxidase from *Scytalidium thermophilum*. *Acta Crystallographica Section D: Biological Crystallography*, 69. 398 - 408. ISSN 0365-110X

<https://doi.org/10.1107/S0907444912049001>

---

**Reuse**

Unless indicated otherwise, fulltext items are protected by copyright with all rights reserved. The copyright exception in section 29 of the Copyright, Designs and Patents Act 1988 allows the making of a single copy solely for the purpose of non-commercial research or private study within the limits of fair dealing. The publisher or other rights-holder may allow further reproduction and re-use of this version - refer to the White Rose Research Online record for this item. Where records identify the publisher as the copyright holder, users can verify any specific terms of use on the publisher's website.

**Takedown**

If you consider content in White Rose Research Online to be in breach of UK law, please notify us by emailing [eprints@whiterose.ac.uk](mailto:eprints@whiterose.ac.uk) including the URL of the record and the reason for the withdrawal request.



[eprints@whiterose.ac.uk](mailto:eprints@whiterose.ac.uk)  
<https://eprints.whiterose.ac.uk/>

## Crystal structure, recombinant expression and mutagenesis studies of the catalase with oxidase activity from *Scytalidium thermophilum*

Yonca Yuzugullu<sup>a</sup>, Chi H. Trinh<sup>b</sup>, Mark A. Smith<sup>c</sup>, Arwen R. Pearson<sup>b</sup>, Simon E.V. Phillips<sup>d</sup>, Didem Sutay Kocabas<sup>e</sup>, Ufuk Bakir<sup>f</sup>, Zumrut B. Ogel<sup>g</sup> and Michael J. McPherson<sup>b\*</sup>

<sup>a</sup>Biology, Kocaeli University, Kocaeli, 41380, Turkey, <sup>b</sup>Astbury Centre for Structural Molecular Biology, University of Leeds, Leeds, LS2 9JT, United Kingdom, <sup>c</sup>Université de Montréal, Montréal, H3T 1J4, Canada, <sup>d</sup>Research Complex at Harwell, Rutherford Appleton Laboratory, Didcot, OX11 0FA, United Kingdom, <sup>e</sup>Food Engineering Department, Karamanoğlu Mehmetbey University, Karaman, 70200, Turkey, <sup>f</sup>Chemical Engineering Department, Middle East Technical University, Ankara, 06531, Turkey, and <sup>g</sup>Food Engineering Department, Middle East Technical University, Ankara, 06531, Turkey

Correspondence email: m.j.mcpherson@leeds.ac.uk

**Keywords:** Catalase, phenol oxidase, *Scytalidium thermophilum*, site-directed mutagenesis

### Synopsis

Catalytic and oxidative activities of catalase from *Scytalidium thermophilum* are likely to be associated with the same haem active centre. The secondary oxidase activity may be a general feature of mono-functional catalases in the absence of hydrogen peroxide. This bifunctionality may provide some advantages for industry if the oxidase activity can be enhanced through engineering or directed evolution.

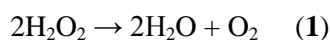
### Abstract

*S. thermophilum* produces a catalase with phenol oxidase activity (CATPO) that catalyses the decomposition of hydrogen peroxide into oxygen and water and also oxidises various phenolic compounds. A codon optimised catpo gene was cloned and expressed in *Escherichia coli*. The crystal structures of native and recombinant *S. thermophilum* CATPO and two variants, H82N and V123F, have been determined at resolutions of 2.7, 1.4, 1.5 and 1.9 Å, respectively. The structure of CATPO reveals a homotetramer with 698 residues per subunit, and strong structural similarity to the

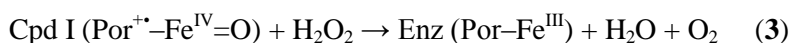
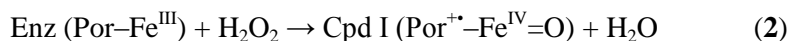
*Penicillium vitale* catalase. The haem component is *cis*-hydroxychlorin  $\gamma$ -spirolactone that is rotated 180° with respect to small subunit catalases. The haem binding pocket contains two highly conserved water molecules on the distal side. The H82N mutation resulted in conversion of the native d-type haem to a b-type haem. Kinetic studies of the H82N and V123F mutants indicate that both activities are likely to be associated with the haem centre and suggest that the secondary oxidase activity may be a general feature of catalases in the absence of hydrogen peroxide.

## 1. Introduction

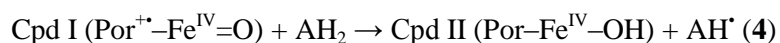
Catalases (hydrogen peroxide: hydrogen peroxide oxidoreductase, EC 1.11.1.6) are haem containing enzymes present in most aerobic organisms (Goldberg & Hochman, 1989; Nicholls et al., 2001). They serve to protect cells against reactive oxygen species by degrading hydrogen peroxide to water and oxygen (Switala & Loewen, 2002; Chelikani et al., 2004; Maté et al., 2001; Nicholls et al., 2001) (scheme 1):



This catalytic reaction occurs in two distinct stages (Chelikani et al., 2004). The first stage involves the oxidation of the haem by the first hydrogen peroxide to form an oxyferryl species and a porphyrin cation radical (scheme 2). In the second stage, this radical intermediate, known as compound I, is reduced by a second hydrogen peroxide to regenerate the resting state enzyme, water and oxygen (scheme 3) (Switala & Loewen, 2002; Nicholls et al., 2001).



At limiting  $\text{H}_2\text{O}_2$  concentrations, and in the presence of a suitable organic donor, catalases may function as peroxidases by catalyzing the one-electron reduction of compound I to form compound II (scheme 4).



The catalase reaction has evolved in four phylogenetically unrelated enzyme classes including the monofunctional or typical catalases, the bifunctional catalase-peroxidases, the non-haem manganese containing catalases and the minor catalases (Maté et al., 2001; Nicholls et al., 2001). The largest and most extensively studied group are the monofunctional catalases, which can be subdivided into those having large (75-84 kDa) subunits and containing haem d or those with small (55-69 kDa) subunits containing haem b. The crystal structures of fourteen monofunctional haem containing catalases from different sources have been reported including bovine liver (Fita et al., 1986; Murthy et al., 1981), *Enterococcus faecalis* (Hakansson et al., 2004), *Escherichia coli* (Bravo et al., 1995; Bravo et al., 1999), *Exiguobacterium oxidotolerans* (Hara et al., 2007; Díaz et al., 2011), *Helicobacter*

pylori (Loewen et al., 2004), human erythrocytes (Ko et al., 1999; Putnam et al., 2000), *Micrococcus lysodeikticus* (Murshudov et al., 1992), *Neurospora crassa* (Díaz et al., 2004), *Penicillium vitale* (Vainshtein et al., 1981; Vainshtein et al., 1986), *Pichia angusta* (Peña-Soler et al., 2011; Díaz et al., 2011), *Proteus mirabilis* (Gouet et al., 1995), *Pseudomonas syringae* (Carpena et al., 2003), *Saccharomyces cerevisiae* (Maté et al., 1999), and *Vibrio salmonicida* (Riise et al., 2007; Díaz et al., 2011). The haem-containing catalases are generally homotetramers having molecular masses ranging from ca. 220 to 330 kDa (Chelikani et al., 2004; Nicholls et al., 2001; Klotz & Loewen, 2003). They exhibit a strong absorbance in the Soret band (406 nm) and have a  $R_z$  (A406/A280) value of around 1 (Zámocký & Koller, 1999). The haem prosthetic groups are either a non-covalently bound iron protoporphyrin IX (haem b) or an oxidised form of protoporphyrin IX (haem d) (Maté et al., 2001). Haem d contains a cis-hydroxy  $\gamma$ -spirolactone that is rotated 180 degrees about the axis defined by the  $\alpha$ - $\gamma$ -meso carbon atoms, when compared with the orientation found for haem b in bovine liver catalase (Fig. 1) (Murshudov et al., 1996). Though the origin of haem d has not been determined it has been suggested that the enzyme is likely to first bind haem b, which is subsequently converted to haem d through oxidation by the first  $H_2O_2$  molecules bound to enzyme (Timkovich & Bondoc, 1990). In hydroperoxidase II this has been shown to be catalyzed by the enzyme itself in the presence of hydrogen peroxide (Maté et al., 2001; Timkovich & Bondoc, 1990; Loewen et al., 1993; Bravo et al., 1997) or singlet oxygen (Díaz et al., 2005) with a requirement of a distal histidine (Loewen et al., 1993).

At low concentrations of hydrogen peroxide some catalases have been shown to possess additional peroxidase activity, demonstrating the ability to oxidise low molecular weight alcohols (Nicholls et al., 2001). In the absence of hydrogen peroxide a further oxidative activity has been documented by Vetrano et al. (2005) for a mammalian catalase. The authors showed that the enzyme oxidised several functionally important phenolic compounds, suggesting a significant biological role for this dual activity (Vetrano et al., 2005). A second example of such a dual-function catalase-oxidase is the bifunctional catalase-phenol oxidase (CATPO) that has been characterised from the thermophilic fungus *S. thermophilum* (Sutay Kocabas et al., 2008). In addition to its major function as a catalase, CATPO also has minor oxidising activity towards various phenolic compounds in the absence of hydrogen peroxide (Sutay Kocabas et al., 2008; Ögel et al., 2006).

*S. thermophilum* CATPO is a homotetramer with a molecular mass of 320 kDa. We have previously reported the crystallization of this enzyme (Sutay Kocabas et al., 2009). Here, we report the crystallographic structure determination of this enzyme at 1.4 Å resolution.

Several residues in the haem pocket are highly conserved amongst haem containing catalases, including an essential distal histidine and valine situated on the distal side of the haem. The histidine is essential for catalysis, acting as an acid-base catalytic group (Loewen et al., 1993), whilst the valine is responsible for narrowing the channel that connects the active site to the exterior of the enzyme

(Maté et al., 1999). In order to begin understanding the basis for the phenol oxidase activity of CATPO we have expressed a codon optimised *catpo* gene from *S. thermophilum* in *E. coli* and have studied two mutant forms of CATPO; H82N and V123F (the essential histidine and valine). Structures of the recombinant wild type (rCATPO) and the two mutants have been determined at 1.4, 1.5 and 1.9 Angstrom resolution, respectively.

## 2. Experimental procedures

### 2.1. Native CATPO expression and purification

Cultures of *S. thermophilum* (type culture *Humicola insolens*, ATCC No. 16454) were grown in modified YpSs growth medium containing 4 g L<sup>-1</sup> yeast extract, 1 g L<sup>-1</sup> K<sub>2</sub>HPO<sub>4</sub>, 0.5 g L<sup>-1</sup> MgSO<sub>4</sub>·7H<sub>2</sub>O, 0.1 g L<sup>-1</sup> CuSO<sub>4</sub>·5H<sub>2</sub>O and 40 g L<sup>-1</sup> glucose. *S. thermophilum* was grown for 5 days at 45 °C with shaking at 155 rpm. Cells were removed by centrifugation at 10,000 rpm for 10 min (4 °C), and the supernatant containing CATPO precipitated with 60% (w/v) ammonium sulphate and dialyzed versus 50 mM Tris-HCl (pH 8.0) overnight at 4 °C. The dialyzed suspension was filtered (0.2 µm) to remove any precipitate before further purification.

*S. thermophilum* CATPO was purified to homogeneity adopting a two-step procedure including anion exchange and gel filtration chromatography using an ÄKTA PRIME FPLC system (Amersham-Pharmacia) at 4 °C. Ion exchange was performed by packing Q Sepharose High Performance medium (GE Healthcare, USA) into a XK 16/20 column (GE Healthcare) followed by equilibration with 50 mM Tris-HCl (pH 8.0) at a flow rate of 1 mL min<sup>-1</sup>. The column was then washed several times with the same buffer and CATPO eluted with a linear gradient from 0-0.4 M NaCl in 50 mM Tris-HCl (pH 8.0). The presence and purity of CATPO was confirmed by SDS-PAGE gel, and combined eluates were dialyzed versus 50 mM Tris-HCl (pH 8.0) alone to remove salt and then concentrated using a 10K centrifugal concentrator (Microsep<sup>TM</sup>, USA) prior to gel filtration. Gel filtration was carried out using a HiPrep 26/60 Sephacryl S-200 high resolution column (GE Healthcare, USA) in 50 mM Tris-HCl (pH 8.0) at a flow rate of 1 mL min<sup>-1</sup>. CATPO containing fractions were pooled and concentrated as before.

### 2.2. *Escherichia coli* strains, media and cultivation

*Escherichia coli* XL-1 Blue (Stratagene) and BL21 Star (DE3) (Invitrogen) strains were used for cloning and expression respectively. During cloning steps *E. coli* were grown aerobically at 37 °C in LB medium supplemented with 50 µg mL<sup>-1</sup> kanamycin.

### 2.3. Molecular cloning

Based on the exon nucleotide sequence of the *S. thermophilum* catalase gene (United States Patent, No. 5646025), an *E. coli* codon optimised sequence of the *catpo* gene coding region was synthesised and cloned into pUC57 (GenScript Corporation, USA) for recombinant expression in *E. coli*. A forward primer (5'-GGAATTCCATATGACCTGCCCGTTCGCTGACCCG-3', 5'-NdeI site is underlined) and a reverse primer (5'-CAAGCTTGGGTTAAGAGTCCAGAGCGAAACGGTC-3', 3'-HindIII site is underlined) were designed to PCR amplify the *catpo* gene from pUC57 excluding the first nineteen codons encoding the N-terminal signal peptide. The cleavage site of the signal peptide was predicted using the SignalP 3.0 server (Bendtsen et al., 2004; Nielsen et al., 1997). The region coding for the mature *catpo* gene was PCR amplified using KOD DNA polymerase (Novagen) under the following conditions: initial denaturing at 95 °C for 2 min; then 30 cycles at 95 °C for 1 min, 70 °C for 1 min, 72 °C for 2.5 min and finally a 10 min extension phase at 72 °C. The PCR product was gel purified (QIAquick gel extraction kit, Qiagen), double restriction digested with NdeI and HindIII (NEB), subcloned into pET28aTEV (kindly provided by Dr. John Taylor and Prof. R.E. Sockett, University of Nottingham) and transformed into competent *E. coli* XL-1 Blue cells. Positive clones were confirmed by restriction analysis and DNA sequencing. The construct, which carried an N-terminal 6x-His tag sequence and TEV protease cleavage site, was designated as pET28a-CATPO.

#### 2.4. Site-directed mutagenesis

Single point mutations were introduced into the *catpo* coding region by QuikChange (Stratagene) using mutagenic primer pairs, substituting Pfu DNA polymerase with KOD DNA polymerase (Novagen) for 30 cycles prior to DpnI digestion. PCR primers containing the desired single mutations (underlined) were as follows (sense only):

5'-CGGAACGTGCTGTAAACGCTCGTGGTGC (H82N) and

5'-CGTTCGTTTCTCTACCTTCGCTGGTTCTCGTGGTTCTGC (V123F).

The introduction of H82N and V123F mutations was confirmed by DNA sequencing.

#### 2.5. Protein over-expression and purification

pET28a-CATPO was freshly transformed into *E. coli* BL21 Star (DE3) and a single colony inoculated into 10 ml LB medium supplemented with 50 µg mL<sup>-1</sup> kanamycin and incubated overnight at 37 °C with shaking (200 rpm). The entire overnight culture was used to inoculate 1 L LB supplemented with 50 µg mL<sup>-1</sup> kanamycin in a 2.4 L conical flask and grown at 37 °C (200 rpm) until an OD<sub>600</sub> of 0.6–0.8, at which point IPTG (0.1 mM, final concentration) was added and incubation was continued at 30 °C (120 rpm) for 24 hr to achieve semi-anaerobic conditions. Cells were then harvested by centrifugation for 10 min at 6,000 rpm (4 °C) and the pellets frozen at -80 °C until use. Following thawing of the pellet, cells were lysed using 100 mL lysis buffer (50 mM NaHEPES, 25% w/v sucrose, 1% v/v Triton-X 100 and 5 mM MgCl<sub>2</sub>·6H<sub>2</sub>O) per L of original culture. The suspension

was centrifuged at 10,000 rpm for 30 min (4 °C) and the supernatant used as either a crude enzyme solution for activity assays or dialyzed overnight versus 20 mM sodium phosphate buffer (pH 7.4), 0.5 M NaCl. The dialyzed fraction was filtered (0.2 µm) and loaded onto a HiTrap Chelating HP (1 mL, GE Healthcare) column pre-charged with Ni<sup>2+</sup> and pre-equilibrated (20 mM sodium phosphate, 0.5 M NaCl 20 mM imidazole, pH 7.4) using a Gradifrac Purifier (GE Healthcare, USA). Recombinant 6xHis–CATPO was purified by affinity chromatography by applying a wash step (20 mM sodium phosphate, 0.5 M NaCl and 100 mM imidazole, pH 7.4) followed by elution collecting 1 mL fractions over a 50 mL linear gradient from 0.1–0.5 M imidazole. Each fraction was tested for purity by SDS–PAGE and the concentration of pooled fractions determined by Bradford assay using bovine serum albumin as a standard.

## 2.6. Enzyme activity assay

Catalase and phenol oxidase activity assays were performed using a temperature-controlled spectrophotometer (Shimadzu UV–2401). All assays were performed in triplicate in 100 mM sodium phosphate buffer (pH 7.0) at 60 °C. Specific activity assays for catalase activity were carried out using 10 mM H<sub>2</sub>O<sub>2</sub> as a substrate and enzyme activity determined using the initial rate of the reaction monitoring the decrease in absorbance at 240 nm ( $\epsilon_{240}$  H<sub>2</sub>O<sub>2</sub> of 39.4 M<sup>-1</sup> cm<sup>-1</sup> (Merle et al., 2007)). One unit of activity was defined as the amount of enzyme that catalysed the decomposition of 1 µmol H<sub>2</sub>O<sub>2</sub> per min. Phenol oxidase activity was determined by monitoring the increase in absorbance at 420 nm using 100 mM catechol as a substrate. Enzyme activity was determined using the initial rate of the reaction and the extinction coefficient at 420 nm of 3450 M<sup>-1</sup>cm<sup>-1</sup> for catechol (Ögel et al., 2006) where one unit of activity corresponded to the formation of 1 nanomole of product per min.

## 2.7. UV-vis spectra

All spectroscopic measurements were performed on a 2401 PC UV/Vis spectrophotometer (Shimadzu) at room temperature. Absorption spectra of purified native, recombinant wild type and mutational variants were recorded in a quartz cuvette (1 cm path length) between 200–900 nm.

## 2.8 Comparison of rCATPO catalase and phenol oxidase activities with catalases from different sources

In addition to purified *S. thermophilum* rCATPO, catalases from four different sources; *A. niger*, human (erythrocytes), *Corynebacterium glutamicum*, and bovine liver were obtained from Sigma-Aldrich, Germany and assayed for catalase and phenol oxidase activity.

## 2.9 Crystallization, data collection and refinement

Crystals of native CATPO, improved in size and diffraction capability with respect to those previously reported (Sutay Kocabas et al., 2009), were obtained at 18 °C with a protein concentration of 9.4 mg mL<sup>-1</sup> using the sitting drop vapour diffusion method over a reservoir solution containing 18% w/v PEG 2000, 0.1 M barium chloride and 0.1 M Bis-Tris (pH 6.8). Prior to flash cooling of the crystal in liquid nitrogen for diffraction analysis, 45% w/v PEG 2000 (final concentration) was added to the mother liquor droplet containing the brownish-green crystals and left overnight to diffuse. Diffraction data were collected using synchrotron radiation at beam line I03 (Diamond Light Source, UK) at a wavelength of 0.97 Å (Table 1). The diffraction data were processed using MOSFLM (Leslie, 1999), scaled with SCALA (Evans, 1997) and reduced using SCALA and TRUNCATE from the CCP4 program suite (Winn et al., 2011). Structure determination of native CATPO was carried out with the program MOLREP (Vagin & Teplyakov, 1997) using the native PVC (*P. vitale* catalase) structure as the search model (PDB code: 2IUF). Model building and refinement were performed using Coot (Emsley et al., 2010) and REFMAC5 (Murshudov et al., 2011) with 4-fold NCS applied.

Diamond shaped crystals of recombinant wild type CATPO (rCATPO) and the H82N variant were obtained by vapour diffusion over reservoirs containing 6–16% w/v PEG 400, 0.2 M potassium chloride, 0.01 M calcium chloride and 0.05 M sodium cacodylate between pH 5.0–5.6. Crystals of V123F were obtained under similar conditions except that PEG 4000 was used as precipitant rather than PEG 400. Good quality crystals were then flash cooled in liquid nitrogen after soaking crystals in 20% v/v PEG 400 (final concentration). The diffraction data were also collected at Diamond Light Source at 100K (Beamlines I02, I04.1 and I04), followed by autoindexing and integration using XDS (Kabsch, 2010). Subsequent steps were carried out using the CCP4 suite (Winn et al., 2011). The crystal structure of V123F was determined using the native structure of *S. thermophilum* catalase as a molecular replacement model. The crystal structure of rCATPO was then determined using the V123F structure as a molecular replacement model and this was then used to phase the H82N variant data.

All figures were prepared using PyMol (<http://pymol.org/>). The structure factors and coordinates have been submitted to the Protein Data Bank with the accession codes 4AUE for native CATPO, 4AUM for rCATPO, 4AUL for H82N and 4AUN for V123F.

### 3 Results

#### 3.8 Characterization of CATPO variants

Recombinant wild-type and the mutational variants of CATPO appeared as single bands at an apparent molecular weight of 79 kDa, as determined by SDS–PAGE (Fig. 2). Both purified native and recombinant CATPO were green in colour, indicative of a d-type haem prosthetic group. The UV–Vis spectrum of native CATPO had absorption maxima at 280, 402, 592 and 691 nm (Fig. 2), with an *R*<sub>z</sub>



value (402/280 nm) of ca. 0.5 that is consistent with the haem content reported previously for native CATPO (Sutay Kocabas et al., 2008). Phenol oxidase activities were approximately the same for native and recombinant CATPO except that recombinant wild-type enzyme exhibited a 2-fold higher catalase activity. UV–Vis spectroscopy of the recombinant wild-type CATPO also showed 4 major peaks at 280, 406, 590, and 714 nm, and consistent with its increased catalase activity, the recombinant enzyme had an increased Rz value of 0.9.

To investigate the basis of the dual functionality of CATPO for phenol oxidation and catalase activities, whether both catalytic reactions occur at the prosthetic haem centre and whether catalysis requires a d-type haem, we generated mutational variants designed to target two conserved residues H82 and V123, both residues of which are conserved in almost all monofunctional catalases (Murshudov et al, 1996). Two variants were generated: H82N and V123F. H82 lies dorsal to the haem d and is absolutely required for activity (Melik-Adamyan et al., 2001). Mutation of this residue in *E. coli* HP11 catalase to Asparagine (Asn) has been shown to result in a b-type protohaem bound in place of the haem d (Obinger et al., 1997). The V123 equivalent residue in the HP11 catalase (V169) lies in the channel above H82 and mutation of this residue in HP11 has been shown to result in a 12-fold reduction in catalase activity whilst retaining haem d (Chelikani et al., 2003).

Purified CATPO H82N was red in colour with an Rz value of 0.8 consistent with that of rCATPO, indicating substantial haem content. CATPO H82N demonstrated extremely low catalase and reduced phenol oxidase activities of 0.02% and 23% compared with that of rCATPO (Table 2). Consistent with its red color, H82N had  $\lambda_{\text{max}}$  values at 280, 406, 536, 629 nm with the absence of the characteristic haem d peak at 590 nm indicating a lack of haem d and presence of (proto)haem b. By contrast, purified V123F CATPO was green in colour, had an identical Rz value to the H82N variant yet displayed identical spectral features to rCATPO with  $\lambda_{\text{max}}$  values at 280, 406, 590, and 714 nm, indicating the presence of haem d. However, both catalytic activities of the V123F variant were substantially reduced to 0.3% catalase activity and 10% phenol oxidase activity relative to rCATPO (Table 2).

### 3.9 Comparison of oxidase activity of catalases from different sources

To examine whether the catalase/phenol oxidase dual activity is a more general property of catalases, four commercially available catalases from *A. niger*, human erythrocyte, *C. glutamicum* and bovine liver were purchased. Human erythrocyte catalase showed the highest enzymatic activity, with *C. glutamicum* the second most active, *S. thermophilum* the third, whilst *A. niger* and bovine liver catalases showed the lowest activities (Table 3).

Surprisingly, all four commercial enzymes showed a phenol oxidase activity when assayed with catechol (Table 3). The phenol oxidase efficiencies of human, bovine liver and *S. thermophilum* catalases were found to be ca. 1.4%, 1.2% and 1.14% respective to their catalase activities, whilst *A.*

niger catalase demonstrated a ca. 50% lower phenol oxidation efficiency than that of *S. thermophilum* at ca. 0.6%. The lowest phenol oxidase active catalase tested was *C. glutamicum* at 0.4%.

### 3.10 Quality of the structural models

The electron density map of the native enzyme defines the main chain and side chain atoms of 2,679 amino acids, 316 water molecules and 21 di-N-acetylglucosamine (NAG) moieties. The map shows clear continuity in all subunits over the backbone chain from Glu27 to Asp697. The twenty-six residues at the N-terminus, predicted from the gene sequence, are disordered in all four subunits. Ser698 in subunits A and C is not modelled due to weak density. The following regions are disordered: Ala618–Ala621 in subunit A and C, Ala618–Thr620 in subunit B and Ala618–Ser622 in subunit D. The final model was refined at 2.7 Å resolution with 4-fold NCS restraints.

The rCATPO structure contains four subunits with 2,694 amino acids, four haem groups and 2,463 water molecules. The map shows continuity in almost all subunits over the complete length from Ser21 to Asp697. Ser698 in all subunits except B is not modelled due to weak density. The following loops are disordered: Phe617–Ser622 in subunits A and B and Ala618–Ser622 in subunits C and D. Aside from the lack of glycosylation, the native and recombinant wild-type CATPO structures have an r.m.s.d. over all atoms of 0.35 Å and are essentially the same. As for the structure of rCATPO, the mutants analysed here, H82N and V123F, are also homotetramers with 2,690 amino acids. Besides similar disordered regions to rCATPO, the loop between residues Gly650 and Val655 could not be modelled due to weak density. The N-terminal 20 residues of all subunits in all three (rCATPO, H82N and V123F) structures are disordered, as in the wild type native enzyme, and are not included in the final refined models. Data and model quality statistics are summarised in (Table 1).

The quality and resolution of the diffraction data are considerably better for rCATPO than for the native protein, therefore the structure of recombinant protein will be further discussed here.

### 3.11 Overall structure

rCATPO crystallizes with a homotetramer in the asymmetric unit in space group C2 and unit cell dimensions of 201.4 Å, 121.4 Å, and 125.2 Å. The rCATPO monomer is similar to that described for other catalases (Bravo et al., 1999; Vainshtein et al., 1986; Díaz et al., 2009) and is composed of five different regions; a long amino-terminal arm, an antiparallel eight-stranded β-barrel, an extended wrapping loop, a four helical domain and, as in large catalases, a carboxy-terminal domain with flavodoxin like topology joined by a long loop (Fig. 3).

rCATPO was purified using an N-terminal His-tag, however, Ser21 is the first residue visible in the crystal structure, suggesting that the N-terminal 20 residues and His-tag are disordered. The amino terminal domain (Ser21 to Glu74) is entirely buried by neighbouring subunits. The haem binding domain is a β-barrel consisting of eight anti-parallel β-strands accompanied by several helical

segments of one to four turns each. The first half of the  $\beta$ -barrel (residues Gly138 to Asn155) is involved in forming the substrate access channel cavity on the distal side of haem. The extended wrapping loop of 64 residues (Pro386 to Arg449) connects the  $\beta$ -barrel and  $\alpha$ -helical regions. This region lacks secondary structure in a long stretch of polypeptide chain between residues 389–442 whilst the remainder comprises mostly  $\alpha$ -helices. Fungal catalases have six or seven prolines in the wrapping loop that in CATPO represent Pro386, cis-Pro416 and cis-Pro424, which also are structurally conserved in PVC (*P. vitale*), HPII (*E. coli*) and CAT-3 (*Neurospora crassa*). Three other prolines Pro390, Pro393 and Pro439 are also conserved in PVC, whereas only one, Pro413, is present in CATPO where this domain ends with a one  $\beta$ -strand close to the  $\alpha$ -helical domain.

The  $\alpha$ -helical domain contains 70 residues (Glu450 to Gly519) forming four anti-parallel contiguous helices ( $\alpha$ 18– $\alpha$ 21) where  $\alpha$ 18 and  $\alpha$ 20 form the site for NADPH binding in small subunit catalases like BLC. However in large subunit catalases like CATPO, the hydrophilic environment of the coil, responsible for connecting into the carboxy-terminal region, prevents NADPH binding (Díaz et al., 2004).

The carboxy-terminal domain has 179 amino acid residues (Ala520 to Ser698) and is highly structured with an  $\alpha/\beta$  arrangement with mainly parallel  $\beta$ -strands in a “flavodoxin-like” topology.

### 3.12 Comparison of CATPO with HPII and PVC

Main chain structural alignment of CATPO, HPII and PVC reveals extensive structural conservation (Fig. 4a). The  $\beta$ -barrel, the wrapping loop, and the  $\alpha$ -helical domain are almost identical in CATPO, HPII and PVC. The major differences between these enzymes are located in the N-terminal and C-terminal regions. HPII has a longer amino-terminal arm than both CATPO and PVC (Fig. 4). The extended nature of the amino-terminal region in HPII has been proposed to be responsible for its enhanced stability at high pH or temperature (Sevinc et al., 1995). This might be due to the additional presence of three helices and two  $\beta$ -sheets in HPII, whereas CATPO has only one  $\alpha$ -helix but no  $\beta$ -sheets.

The carboxy-terminal domain of large catalases has low sequence similarity but a conserved general structure (Supplementary Figure 1). PVC and HPII have 9 amino acid residues more than CATPO and in HPII the C-terminal end has a different orientation than in CATPO and PVC.

### 3.13 Haem pocket

The four haem molecules are deeply buried inside the CATPO tetramer at about 22 Å from the nearest solvent exposed surface, as in other haem-containing catalases whose structures have been determined (Maté et al., 2001; Loewen, 1997). The haem lies between the  $\beta$ -barrel ( $\beta$ 1– $\beta$ 4) and helices  $\alpha$ 4 and  $\alpha$ 14 (Fig. 3). In CATPO, as in other catalases, the propionic acids of the haem make salt bridges with three conserved arginine residues (Arg79, Arg119 in  $\beta$ 2 and Arg365 in  $\alpha$ 14).

As in PVC and HP11, the haem d group identified in the active centre of CATPO has a cis-hydroxy  $\gamma$ -spirolactone structure, which can be clearly observed in the electron density map. The presence of the  $\gamma$ -spirolactone ring and hydroxyl group make the haem d more asymmetric with respect to the haem b found in small clade 3 catalases.

On the proximal side of the haem, Tyr369 forms the fifth coordination bond to the iron. There does not appear to be a direct coordination of water with the iron in the sixth coordination position because the closest water molecule is 2.3 Å away in all subunits. This is consistent with the spectral data reported here and for other haem-d catalases that indicates these enzymes contain a 5-coordinate high spin ferric iron (Loewen et al., 2004). The tyrosine phenolate also makes a hydrogen bond with Arg365 (Fig. 5). On the distal side, the imidazole ring of His82 lies almost parallel to the haem above the pyrrole ring IV. The N $\delta$  atom of His82 forms a hydrogen bond with the Ser121 hydroxyl. The N $\epsilon$  atom of this essential histidine also forms a hydrogen bond with a water molecule (W2). As observed in other large catalases, His82 is stabilised by Arg119 and Val123 through hydrogen bonds with its main chain oxygen and nitrogen, respectively (Fig. 5).

The water molecules, W1 and W2, are bound to either the haem or amino acid residues of the haem pocket. W1 interacts with the two haem propionic acid groups while W2 interacts with the N $\epsilon$  atom of His82 and water molecules W1 and W3. Three other water molecules (W9–W11) are located in the channel leading away from the haem pocket towards the protein surface. Two are close to the amino-terminal arm and one is in the carboxy-terminal region (Fig. 5).

### 3.14 Structural differences of the CATPO variants with respect to the wild type enzyme

The three dimensional structures of H82N and V123F variants of CATPO were determined and refined at 1.5 and 1.9 Å resolution, respectively. In contrast to the native CATPO, rCATPO and H82N crystal forms, the V123F crystals contain one tetramer and two dimers in each asymmetric unit. The dimers are part of tetramers that lie on the crystallographic 2-fold axis. The final refined structures provided a clear electron density map that revealed significant differences in both the variant residue and the haem group with respect to wild type CATPO.

The most obvious change in the structure of the H82N is the presence of haem b, as suggested by the spectral analysis (Fig. 6). Substitution of the imidazole ring for an amide group increases the size of the cavity above the haem, whereby W1 moves towards side chain of Asn82 to make a hydrogen bond. W1 is also hydrogen bonded to new water, WA, which is not observed in the wild type enzyme. The propionate group from ring III of the unmodified haem b is hydrogen bonded with the nearby Gln373 and Arg376 residues, which also interact with an adjacent W5. Changing Val123 to the bulky side chain of phenylalanine reduces the size of the distal cavity displacing several water molecules as it interposes between W2 and W10 and breaking the hydrogen bond to His82. Purified V123F

exhibited low catalytic activity, consistent with the larger side chain interfering with substrate access to the active site. The structure also confirms that conversion from haem b to haem d had occurred.

#### 4 Discussion

We have developed a recombinant expression system that allows efficient intracellular production of CATPO in *E. coli*. The UV–Vis spectrum of recombinant CATPO exhibited absorption maxima similar to native CATPO and to *E. coli* HPII catalase that indicated the presence of haem d (Loewen et al., 1993). Haem d-containing catalases contain a high spin ferric [Fe(III)] system five coordinate iron centre consisting of the porphyrin ring and a proximal tyrosine coordinated from the polypeptide. The observed CATPO absorbance bands at ca. 590 and 708 nm bands are indicative of high spin Fe(III) species. The spectral data for both the recombinant wild-type and the H82N and V123F variants, normalised to the main Soret absorption peak at 406 nm, revealed that the recombinant enzymes exhibit a Soret band ratio ( $A_{406}/A_{280} = 0.8$  to  $0.9$ ) indicative of a higher haem content than in the native enzyme ( $A_{402}/A_{280} = 0.5$ ). Thus, native CATPO seems to be deficient in haem d, perhaps having only ca. 2 moles of haem d per mole tetramer. Surprisingly, given the low haem content of the purified native CATPO, the B factors for the haem in the native structure are similar to those of the surrounding protein suggesting that, in the crystals, the haem is present at full occupancy. It is possible that a modification to the haem such as a crosslink might result in a perturbation of its spectral properties, as has been reported for the I274C mutant of KatE which contains a cys-haem crosslink (Jha et al., 2011). However, there is no evidence for any covalent modification of the haem in the native CATPO structure.

A more likely hypothesis to explain the apparent discrepancy between the low haem content in solution and the full occupancy in the crystal is that crystallization preferentially selects the haem containing form. The structure of a recombinant catalase depleted in iron has been reported (Andreoletti et al., 2003) suggesting that catalase can fold in the absence of iron, as long as the porphyrin is present. Interestingly in this case crystallization also appeared to preferentially select the mature haem containing protein as the iron occupancy in the structure was refined to 60%, whereas the mature haem content measured by pyridine hemochromogen was only ~ 30%. The most likely scenario here therefore appears to be that the purified native CATPO is somewhat deficient in haem content, resulting in a low  $R_z$  value, but that crystallization selects out the haem containing, and possibly more stable, CATPO.

When this enzyme was first isolated it was identified that production of active CATPO was enhanced by the addition of copper, suggesting that perhaps the catalase and phenol oxidase activities occurred at distinct sites, a haem and a copper centre, respectively (Ögel et al., 2006). We see no evidence in the crystal structure for any non-haem prosthetic group. In order to test whether the haem group is indeed the redox centre for both catalase and phenol oxidase activities we investigated two

active site mutations. In other mono-functional catalases, these mutations have been shown to affect H<sub>2</sub>O<sub>2</sub> binding and the type of haem incorporated (Loewen et al., 1993; Melik-Adamyany et al., 2001, Chelikani et al., 2003).

In the V123F variant, which contains haem d, the larger phenyl side chain was introduced to reduce the size of the substrate binding channel. As expected, this results in a marked reduction in catalase activity (0.3%). This variant also shows reduced phenol oxidase (10%) activity. The V123F mutation potentially acts in two ways. It probably sterically hinders access of peroxide or oxygen to the active site and reduces the polarity of the active site due to the displacement of waters, resulting in a less favourable environment for activated oxygen species. A second mutation, that of the conserved histidine (H82) to asparagine, has also been reported to perturb the haem active site by preventing conversion of haem b to haem d (Loewen et al., 1993). As expected, in this study the H82N variant contained haem b and displayed very low catalase activity (0.02%). In this case, dioxygen access to the active site is unhindered, however the shorter asparagine side chain is presumably less able to steer productive binding and activation. This may alter the relative efficiencies of the catalase and oxidase activities, reflected in a less marked effect on phenol oxidase activity (23%).

These data are consistent with the haem group acting as the redox centre for both catalase and phenol oxidase activities. However, while both mutations severely affect the catalase activity, appreciable oxidase activity remains. This suggests that the binding site for oxidase substrates is not directly at the haem but is rather, as previously proposed, at a site linked to the haem by an electron transfer pathway (Sicking et al., 2008, Olson & Bruce, 1995). In mammalian NADP(H) binding catalases the NADPH, which binds in a pocket > 10 Å away from the haem, has been proposed to either prevent formation of the inactive compound II or to reduce compound I under low H<sub>2</sub>O<sub>2</sub> conditions to reduce the risk of damage to the catalase active site (Kirkman and Gaetani, 2007). It is possible the PO activity is fulfilling a similar role, but at such a low rate that the higher haem content of the recombinant protein does not have a significant effect on the observed PO rate.

The structure of CATPO shows a high degree of structural similarity to previously determined catalase structures. This supports our previous work (Sutay Kocabas et al., 2008) demonstrating that, in the presence of H<sub>2</sub>O<sub>2</sub>, catalase activity dominates. However, in the absence of H<sub>2</sub>O<sub>2</sub>, there is clear evidence for a low level of phenol oxidase activity (Sutay Kocabas et al., 2008) suggesting that in vivo phenolic substrates will be oxidised in the presence of oxygen. It is not possible at this stage to determine the biological significance of the phenol oxidase activity. This oxidase activity has also been shown to occur in other catalases. Vetrano et al. (2005) demonstrated oxidase activity in a range of mammalian catalases, including those from bovine and mouse liver, mouse and human keratinocytes and fibroblasts, as well as from purified enzyme preparations. We have also demonstrated phenol oxidase activity in CATPO, and in various commercially available catalase samples from human erythrocyte, bovine liver, *C. glutamicum*, as well as from another fungal source

*A. niger*. We speculate that this secondary oxidase activity may be a general feature of some, if not all, catalases but that in most cases it has not been detected due to its relatively low level and indeed the fact that most work on these enzyme has focused on their primary catalase activity.

Our recombinant expression system and new structural models provide a sound basis for further structure-based studies to further dissect the two distinct catalytic activities of this bifunctional fungal enzyme. We anticipate that such studies will provide information that translates to a wide number of catalases from diverse sources. Bifunctionality may also provide some advantages for industrial applications such as detoxification and/or in the action of chemoprotective agents, particularly if the oxidase activity can be enhanced through engineering or directed evolution.

We would like to thank the Middle East Technical University (BAP-08-11-DPT2002K120510), ÖYP-DPT, the Biotechnology and Biological Research Council for funding (MJM and SEVP) and TUBITAK (IPDRFP-2219). We are also grateful to Prof. R.E. Sockett and Dr. John Taylor (University of Nottingham) for providing vector pET28aTEV.

**References**

- Andreoletti, P., Sainz, G., Jaquinod, M., Gagnon, J. & Jouve, H. M. (2003). *Proteins* **50**, 261–71.
- Bendtsen, J. D., Nielsen, H., von Heijne, G. & Brunak, S. (2004). *J. Mol. Biol.* **340**, 783–95.
- Bravo, J., Fita, I., Ferrer, J. C., Ens, W., Hillar, A., Switala, J. & Loewen, P. C. (1997). *Protein Sci.* **6**, 1016–1023.
- Bravo, J., Mate, M. J., Schneider, T., Switala, J., Wilson, K., Loewen, P. C. & Fita, I. (1999). *Proteins* **34**, 155–66.
- Bravo, J., Verdaguer, N., Tormo, J., Betzel, C., Switala, J., Loewen, P. C. & Fita, I. (1995). *Structure* **3**, 491–502.
- Carpena, X., Soriano, M., Klotz, M. G., Duckworth, H. W., Donald, L. J., Melik-Adamyanyan, W., Fita, I. & Loewen, P. C. (2003). *Proteins* **50**, 423–436.
- Chelikani, P., Carpena, X., Fita, I. & Loewen, P. C. (2003). *J. Biol. Chem.* **278**, 31290–31296.
- Chelikani, P., Fita, I. & Loewen, P. C. (2004). *CMLS Cell Mol. Life Sci.* **61**, 192–208.
- Díaz, A., Horjales, E., Rudiño-Piñera, E., Arreola, R. & Hansberg, W. (2004). *J. Mol. Biol.* **342**, 971–985.
- Díaz, A., Muñoz-Clares, R. A., Rangel, P., Valdés, V. J. & Hansberg, W. (2005). *Biochimie* **87**, 205–214.
- Díaz, A., Valdés, V. J., Rudiño-Piñera, E., Horjales, E. & Hansberg, W. (2009). *J. Mol. Biol.* **386**, 218–32.
- Díaz, A., Loewen, P. C., Fita, I. & Carpena, X. (2012). *Arch. Biochem. Biophys.* **525**, 102–110.
- Emsley, P., Lohkamp, B., Scott W. G. & Cowtan, K. (2010). *Acta Crystallogr.* **D66**, 486–501.
- Engh, R. A. & Huber, R. (1991). *Acta Crystallogr.* **A47**, 392–400.
- Evans, P. R. (1997). *Joint CCP4 and ESF-EACBM Newsletter* **33**, 22–24.
- Evans, P. R. (2011). *Acta Crystallogr.* **D67**, 282–292.
- Fita, I., Silva, A. M., Murthy, M. R. N. & Rossmann, M. G. (1986). *Acta Crystallogr.* **B42**, 497–515.
- Goldberg, I. & Hochman, A. (1989). *Biochem. Biophys. Acta* **991**, 330–336.
- Gouet, P., Jouve, H. M. & Dideberg, O. (1995). *J. Mol. Biol.* **249**, 933–954.
- Hakansson, K.O., Brugna, M. & Tasse, L. (2004). *Acta Crystallogr.* **D60**, 1374–1380.
- Hara, I., Ichise, N., Kojima, K., Kondo, H., Ohgiya, S., Matsuyama, H. & Yumoto, I. (2007). *Biochemistry* **46**, 11–22.
- Jha, V., Chelikani, P., Carpena, X., Fita, I., Loewen, P. C. (2012). *Arch. Biochem. Biophys.* **526**, 54–59.
- Kabsch, W. (2010). *Acta Crystallogr.* **D66**, 125–132.
- Kirkman, H. N. and Gaetani, G. F. (2007) *Trends in Biochemical Sciences*, **32**, 44-50
- Klotz, M. G. & Loewen, P. C. (2003). *Mol. Biol. Evol.* **20**, 1098–1112.



- Ko, T. P., Safo, M. K., Musayev, F. N., Di Salvo, M. L., Wang, C., Wu, S. H. & Abraham, D. J. (1999). *Acta Crystallogr.* **D56**, 241–245.
- Leslie, A. G. W. (1999). *Acta Crystallogr.* **D55**, 1696–1702.
- Loewen, P. C., Carpena, X., Rovira, C., Ivancich, A., Perez-Luque, R., Haas, R., Odenbreit, S., Nicholls, P. & Fita, I. (2004). *Biochemistry* **43**, 3089–3103.
- Loewen, P. C., Switala, J., von Ossowski, I., Hillar, A., Christie, A., Tattrie, B. & Nicholls, P. (1993). *Biochemistry* **32**, 10159–10164.
- Lovell, S. C., Davis, I. W., Arendall, W. B. 3rd, de Bakker, P. I., Word, J. M., Prisant, M. G., Richardson, J. S. & Richardson, D. C. (2003). *Proteins* **50**, 437–450.
- Maté, M., Murshudov, G., Bravo, J., Melik-Adamyán, W., Loewen, P. C. & Fita, I. (2001). *Encyclopedia of Inorganic and Bioinorganic Chemistry*, edited by R. A. Scott, pp. 486–502. New York: J. Wiley & Sons Press.
- Maté, M. J., Zamocky, M., Nykyri, L. M., Herzog, C., Alzari, P. M., Betzel, C., Koller, F. & Fita, I. (1999). *J. Mol. Biol.* **286**, 135–139.
- Melik-Adamyán, W., Bravo, J., Carpena, X., Switala, J., Maté, M. J., Fita, I. & Loewen, P. C. (2001). *Proteins* **44**, 270–281.
- Merle, P. L., Sabourault, C., Richier, S., Allemand, D. & Furla, P. (2007). *Free Radic. Biol. Med.* **42**, 236–246.
- Murshudov, G. N., Grebenko, A. I., Barynin, V., Dauter, Z., Wilson, K. S., Vainshtein, B. K., Melik-Adamyán, W., Bravo, J., Ferrá'n, J. M., Ferrer, J. C., Switala, J., Loewen, P. C. & Fita, I. (1996). *J. Biol. Chem.* **271**, 8863–8868.
- Murshudov, G. N., Melik-Adamyán, W. R., Grebenko, A. I., Barynin, V. V., Vagin, A. A., Vainshtein, B. K., Dauter, Z. & Wilson, K. (1992). *FEBS Lett.* **312**, 127–131.
- Murshudov, G. N., Skubak, P., Lebedev, A. A., Pannu, N. S., Steiner, R. A., Nicholls, R. A., Winn, M. D., Long, F. & Vagin, A. A. (2011). *Acta Crystallogr.* **D67**, 355–367.
- Murthy, M. R. N., Reid, T. J., Sicignano, A., Tanaka, N., & Rossmann, M. G. (1981). *J. Mol. Biol.* **152**, 465–499.
- Nicholls, P., Fita, I. & Loewen, P. C. (2001). *Adv. Inorg. Chem.* **51**, 51–106.
- Nielsen, H., Engelbrecht, J., Brunak, S. & von Heijne, G. (1997). *Protein Eng.* **10**, 1–6.
- Obinger, C., Maj, M., Nicholls, P. & Loewen, P. C. (1997). *Arch. Biochem. Biophys.* **342**, 58–67.
- Ögel, Z. B., Yüzügüllü, Y., Mete, S., Bakir, U., Kaptan, Y., Sutay, D. & Demir, A. S. (2006). *Appl. Microbiol. Biotechnol.* **71**, 853–862.
- Olson, L. P., Bruice, T. C., (1995) *Biochemistry* **34**, 7335–7347
- Peña-Soler, E., Vega, M. C., Wilmanns, M. & Williams, C. (2011). *Acta Crystallogr.* **D67**, 690–698.
- Putnam, C. D., Arvai, A. S., Bourne, Y. & Tainer, J. A. (2000). *J. Mol. Biol.* **296**, 295–309.

- Riise, E. K., Lorentzen, M. S., Helland, R., Smalås, A. O., Leiros, H. - K. S. & Willassen, N. P. (2007). *Acta Crystallogr.* **D63**, 135–148.
- Sevinc, M. S., Ens, W. & Loewen, P. C. (1995). *Eur. J. Biochem.* **230**, 127–132.
- Sicking, W. Korth, H-G., de Groot, H., Sustmann, R. (2008) *J. Am. Chem. Soc.* **130**, 7345-7356
- Sutay Kocabas, D., Bakir, U., Phillips, S. E. V., McPherson, M. J. & Ogel, Z. B. (2008). *Appl. Microbiol. Biotechnol.* **79**, 407–415.
- Sutay Kocabas, D., Pearson, A. R., Phillips, S. E. V., Bakir, U., Ogel, Z. B., McPherson, M. J. & Trinh, C. (2009). *Acta Crystallogr.* **F65**, 486–488.
- Switala, J. & Loewen, P. C. (2002). *ABB Arch. Biochem. Biophys.* **401**, 145–154.
- Timkovich, R. & Bondoc, L. L. (1990). *Adv. Biophys. Chem.* **1**, 203–247.
- Vagin, A. & Teplyakov, A. (1997). *J. Appl. Crystallogr.* **30**, 1022–1025.
- Vainshtein, B. K., Melik-Adamyan, W. R., Barynin, V. V., Vagin, A. A. & Grebenko, A. I. (1981). *Nature* **197**, 411–412.
- Vainshtein, B. K., Melik-Adamyan, W. R., Bajyuiu, V. V., Vagiui, A. A., Grbcuko, A. I., Borisov, V. V., Bartels, K. S., Fita, I. & Rossmann, M. G. (1986). *J. Mol. Biol.* **188**, 49–61.
- Vetrano, A. M., Heck, D. E., Mariano, T. M., Mishin, V., Laskin, D. L. & Laskin, J. D. (2005). *J. Biol. Chem.* **280**, 35372–35381.
- Winn, M. D., Ballard, C. C., Cowtan, K. D., Dodson, E. J., Emsley, P., Evans, P. R., Keegan, R. M., Krissinel, E. B., Leslie, A. G. W., McCoy, A., McNicholas, S. J., Murshudov, G. N., Pannu, N. S., Potterton, E. A., Powell, H. R., Read, R. J., Vagin, A. & Wilson, K. S. (2011). *Acta Crystallogr.* **D67**, 235–242.
- Zámocký, M. & Koller, F. (1999). *Progr. Biophys. Mol. Biol.* **72**, 19–66.

**Figure 1** Structures of (a) haem b and (b) haem d.

**Figure 2** (a) UV-vis spectrum of native CATPO from *S. thermophilum*. (b) Comparison of UV-vis spectra of rCATPO, H82N and V123F variants. Inset: Coomassie stained SDS-PAGE gel showing the purity of CATPO variants.

**Figure 3** Structure of rCATPO tetramer (a), monomer (b) and active centre (c). The haem is coloured green, Tyr369 magenta, His82 gray, Asn155 purpleblue, Val123 red, Phe160 lemon, Phe161 yellow and Phe168 orange.

**Figure 4** Comparison of *S. thermophilum* CATPO, *P. vitale* catalase and HP11 catalase structures. View of chain A of HP11 (PDB Code: 1GGE) and PVC (PDB Code: 2IUF) superposed onto rCATPO (PDB Code: 4AUM). Light pink (*S. thermophilum*), Blue (*P. vitale*), Pale green (HP11), Green (haem centre), Red (Tyrosine 369).

**Figure 5** The haem environment of *S. thermophilum* CATPO. The catalytically important residues His82, Asn155, Ser121, and Val123 on the haem distal side are shown. Also displayed are the conserved residues lining the channel, Arg119, Asp135, Phe160, Phe161, and Phe168. The image shows the conserved residues Pro310, Leu361, Arg365, and Tyr369 on the proximal side. Hydrogen bonds are shown as dashed lines.

**Figure 6** The water distribution in the main channel of rCATPO (a), the H82N variant (b), and the V123F variant (c). The 2Fo-Fc electron density corresponding to the individual water molecules is drawn at 1 RMS and shown as a blue wire mesh.

**Table 1** Crystallographic data collection and refinement statistics.

	S. thermophilum CATPO	rCATPO	H82N	V123F
PDB accession code	4AUE	4AUM	4AUL	4AUN
Diamond beamline	IO3	IO4-1	IO2	IO4
Wavelength (Å)	0.97	0.92	0.98	0.95
Space group	P2 <sub>1</sub> 2 <sub>1</sub> 2	C2	C2	C2
a (Å)	185.4	201.4	201	253.3
b (Å)	216.3	121.4	121.9	243.4
c (Å)	68.6	125.2	124.9	97.1
Resolution (Å)	141.4-2.7 (2.77-2.7)	113.0-1.4 (1.44-1.4)	28.96-1.5 (1.54-1.5)	69.94-1.9 (1.97-1.9)
R <sub>merge</sub> (%)§*	9.8(45)	7.2(43.4)	5.9(44.4)	12.6(53.9)
R <sub>p.i.m.</sub> (%)†*	4.1(19)	2.9(17.3)	5.4(40.5)	8.2(34.7)
Observed reflections	50325	3598880	787895	1485328
Unique reflections	76826	506416	417266	444158
Completeness (%) <sup>*</sup>	99.9(100)	95.3(94.7)	96.4(97.2)	99.8(100.0)
Multiplicity <sup>*</sup>	6.5(6.6)	7.1(7.1)	1.9(1.8)	3.3(3.3)
<I>/σ <sup>*</sup>	13.3(4.0)	16.2(4.4)	6.0(1.8)	7.6(2.4)
<b>Refinement</b>				
R <sub>factor</sub> (%)	19.2(28.5)	11.8(17.1)	14.3(25.0)	16.4(24.6)
R <sub>free</sub> (%) †	25.1(34.9)	14.5(21.2)	19.3(32.1)	20.0(29.1)
No. of protein atoms	21,017	22,242	21,715	42,801
No. of solvent molecules	316	2,463	2,497	3,405
No. of ligand atoms	471	176	172	361
Average overall B-factor (Å <sup>2</sup> )	49	13.2	13.6	15.3
RMS bond lengths (Å) ξ	0.011	0.010	0.016	0.006
RMS bond angles (°) ξ	1.6	1.5	1.9	1.1
<b>Ramachandran analysis, the percentage of residues in the regions of plot (%) ‡</b>				
Most favoured	95	97	96	96
Outliers	0.3	0.5	0.6	0.5

\* Values given in parentheses correspond to those in the outermost shell of the resolution range.

$$\S R_{\text{merge}} = \frac{\sum_{\text{hkl}} \sum |I_i(\text{hkl}) - \langle I(\text{hkl}) \rangle|}{\sum_{\text{hkl}} \sum I_i(\text{hkl})}$$

+ R<sub>pim</sub> - precision-indicating (multiplicity-weighted) R<sub>merge</sub>, relative to I+ or I-.

† R<sub>free</sub> was calculated with 5% of the reflections set aside randomly.

ξ Based on the ideal geometry values of Engh & Huber (1991).

‡ Ramachandran analysis using the program MolProbity (Lovell et al., 2003).

**Table 2** Specific activities of purified CATPO variants.

Variant	Specific Activity	
	Catalase ( $\mu\text{mol mg}^{-1} \text{min}^{-1}$ )	Phenol oxidase ( $\text{nmol mg}^{-1} \text{min}^{-1}$ )
<i>S. thermophilum</i> CATPO	8,870 $\pm$ 1,000	194 $\pm$ 5
rCATPO	18,713 $\pm$ 935	213 $\pm$ 5
H82N	4 $\pm$ 0.6	50 $\pm$ 13
V123F	65 $\pm$ 6	22 $\pm$ 1

**Table 3** Comparison of CATPO catalase (CAT) and phenol oxidase (PO) activities with other catalases.

Catalase Source	CAT Activity ( $\mu\text{mol mg}^{-1} \text{min}^{-1}$ )	PO Activity ( $\text{nmol mg}^{-1} \text{min}^{-1}$ )
rCATPO	18,713 $\pm$ 935	213 $\pm$ 5
<i>A. niger</i>	3,502 $\pm$ 321	20 $\pm$ 0.4
<i>C. glutamicum</i>	53,315 $\pm$ 692	204 $\pm$ 4
Bovine liver	6,125 $\pm$ 1027	73 $\pm$ 1.6
Human erythrocyte	98,477 $\pm$ 4652	1,342 $\pm$ 25